



## Article

# Artificial Structures Steer Morphological Development of Salt Marshes: A Model Study

Rutger W. A. Siemes <sup>1,2,\*</sup> , Bas W. Borsje <sup>1</sup>, Roy J. Daggen Voorde <sup>2</sup> and Suzanne J. M. H. Hulscher <sup>1</sup> 

<sup>1</sup> Water Engineering & Management, University of Twente, P.O. Box 217, 7500 AE Enschede, The Netherlands; b.w.borsje@utwente.nl (B.W.B.); s.j.m.h.hulscher@utwente.nl (S.J.M.H.H.)

<sup>2</sup> HKV Consultants, P.O. Box 2120, 8203 AC Lelystad, The Netherlands; r.daggen Voorde@hkv.nl

\* Correspondence: r.w.a.siemes@utwente.nl

Received: 3 April 2020; Accepted: 28 April 2020; Published: 5 May 2020



**Abstract:** Salt marshes are increasingly recognized as resilient and sustainable supplements to traditional engineering structures for protecting coasts against flooding. Nevertheless, many salt marshes face severe erosion. There is a consensus that providing structures that create sheltered conditions from high energetic conditions can improve the potential for salt marsh growth. However, little proof is provided on the explicit influence of structures to promote salt marsh growth. This paper investigates how artificial structures can be used to steer the morphological development of salt marshes. A morphological model (Delft3D Flexible Mesh) was applied, which enabled the analysis of various artificial structures with realistic representation. A salt marsh in the Wadden Sea which has seen heavy erosion (lateral retreat rate of 0.9 m/year) served as case study. We simulate both daily and storm conditions. Hereby, vegetation is represented by an increased bed roughness. The model is able to simulate the governing processes of salt marsh development. Results show that, without artificial structures, erosion of the salt marsh and tidal flat continues. With structures implemented, results indicate that there is potential for salt marsh growth in the study area. Moreover, traditional structures, which were widely implemented in the past, proved to be most effective to stimulate marsh growth. More broadly, the paper indicates how morphological development of a salt marsh can be steered by various configurations of artificial structures.

**Keywords:** salt marsh; Wadden Sea; nature-based coastal protection; artificial structures; coastal resilience; numerical modeling; process-based

## 1. Introduction

Salt marshes are vegetated foreshores which occur at sheltered muddy coastlines in temperate latitudes. These vegetated foreshores have the ability to attenuate waves and stabilize the bed [1,2]. Furthermore, research has indicated that they are able, within limits, to keep up with a rising sea level [3]. Vuik et al. [4] showed that stimulating marsh growth can reduce initial costs for improving coastal safety by a factor 10 compared to dike heightening. However, stimulating marsh growth does bring about maintenance costs. In addition to providing coastal-safety benefits, they also provide ecological benefits by supporting more diverse biota [5]. Moreover, they are able to sequester carbon with 2.1 Mg ha<sup>-1</sup> yr<sup>-1</sup> on average [6] compared to 0.2–0.6 Mg ha<sup>-1</sup> yr<sup>-1</sup> for grasslands [7]. In addition, they are able to treat waste with a factor 75 compared to grasslands and forests which makes salt marshes among the most valuable ecosystems on earth [8]. In light of these characteristics, stimulation of salt marsh growth can offer a resilient and sustainable supplement to traditional engineering structures for protecting coasts against flooding.

Though the benefits of vegetated foreshores are increasingly recognized, many foreshores, including salt marshes, suffer erosion [9,10]. While the erosion rate of a salt marsh cliff (typically tens of centimeters in height) exhibits a linear relation with wave power [11], the start of erosion is linked to having a stable marsh next to a dynamic tidal flat. Consequently, a cliff can develop at the marsh front which is attacked by wave action resulting in erosion [12].

Conversely, the start of salt marsh expansion is characterized by seedling establishment or clonal shoots. Hereby, vegetation stabilizes the bed and functions as a sediment trap. For seedling establishment to succeed, conditions should be such that uprooting or burying of the seedlings is prevented [13]. The indicating parameters for these conditions are the bed elevation in relation to water level (influencing inundation frequency and period), and bed level change. Clonal expansion is affected mainly by inundation period and wave and flow energy at the tidal flat [14]. The start of salt marsh growth can thus be stimulated by improving the aforementioned conditions at the tidal flat in front of the marsh, for either clonal shoots or seedling establishment.

Thus, creating an area sheltered from high energy conditions can improve the potential for vegetation establishment and hence for salt marsh growth [15]. However, little research is performed on how human interventions can be applied to promote salt marsh growth. Van Loon-Steensma and Slim [16] investigated the biodiversity that occurs on salt marshes which are restored with the aid of groynes. In addition, the long-term cost effectiveness of ecological engineering methods for vegetated foreshores are assessed by Vuik et al. [4]. In this study, bed level changes on the foreshore are based on spatially uniform accretion scenarios. Dao et al. [17] investigated the wave-damping effect of brushwood groynes, structures often applied to stimulate salt marsh growth. However, research on implementing artificial structures to influence morphological development of salt marshes is still lacking. Recently, Vona et al. [18] analyzed the hydrodynamics and morphodynamics on and around a salt marsh after the implementation of breakwaters. Their research indicates the potential of wave damping to protect shorelines, but also that structures can block sediment transport, negatively affecting marsh growth.

Research on the morphological development of vegetated foreshores is performed by field or modeling studies. While field studies can give detailed insight into the conditions that cause bed level change [2,19], this method can be expensive and does not lend itself well for to the study of long-term morphological developments. Morphological models can be used to study these long-term developments. Moreover, with the ability to alter input characteristics, the impact of individual processes and varying scenarios can be analyzed efficiently [15,20]. Similarly, modeling also offers the possibility to assess a range of configurations of artificial structures as well.

The aim of this paper is to investigate how artificial structures can be applied to steer the morphological development of salt marshes. This will be achieved by, (1) analyzing the dynamic processes motivating morphological development on and around a salt marsh and (2) studying the impact of human interventions on these processes. A process-based numerical model is developed in Delft3D Flexible Mesh (D3D-FM), in which accurate bed levels and hydrodynamic forcing are applied to simulate a month with both daily conditions and storm conditions. A small salt marsh in the Wadden Sea is selected as the case study. This marsh has suffered heavy erosion (lateral retreat rate of  $0.9\text{ m/year}$ ) since maintenance of its sedimentation fields and groyne was halted. In addition, based on local flow and sediment characteristics, salt marsh stimulation here is expected to require large efforts within the area [21].

The outline of this paper is as follows. Section 2 describes the study area and the setup of the morphological model applied within this study. In Section 3, the hydrodynamic results are presented and validated after which the morphological results are presented. Next, results including human interventions are presented. Consequently, in Section 4, the assumptions and uncertainties within the model setup are discussed, after which we will discuss the results. The applicability of this paper is also addressed. In Section 5, the conclusions are presented.

## 2. Materials and Methods

### 2.1. Study Area and Field Observations

The study area is located in the Wadden Sea, south of the tidal inlet between Ameland and Schiermonnikoog (Figure 1b). The study area contains a salt marsh and the tidal flat in front of the marsh, up to 1 km seawards (Figure 1c). Hereby, and throughout this paper, the salt marsh is denoted as the part of the study area with a bed level above 0.7 *m N.A.P.*, the marsh front is the area of the marsh with a bed level between 0.7–1.2 *m N.A.P.* (Amsterdam Ordnance Datum or Normaal Amsterdams Peil). The tidal flat includes the rest of the study area, up to 1 km away from the shore.

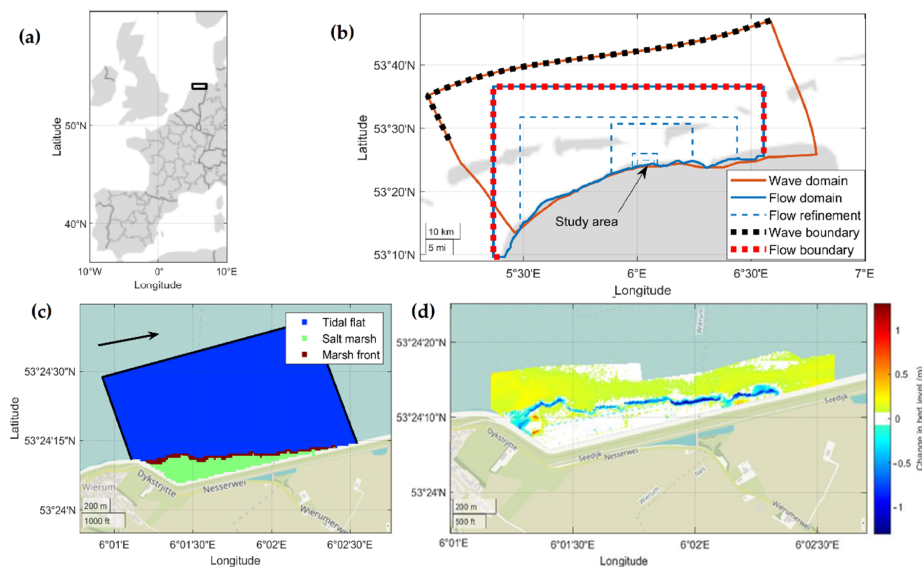


**Figure 1.** (a) The study area’s location within Europe. (b) The area of the model domains and their main characteristics. The arrow indicates the location of the study area, which is the salt marsh near Wierum, the Netherlands. (c) The location of the tidal flat, salt marsh, and marsh front within the study area. The marsh front is also part of the salt marsh itself. The arrow indicates the dominant direction of tidal flow and alongshore transport. (d) Observed bed level change between the spring of 2008 and the spring of 2014 [22]. The erosion in dark blue displays the erosion of the marsh edge.

Tides in the area are predominantly semi-diurnal with an averaged amplitude of 1.1 *m*. The amplitude of a spring-neap cycle, on top of the average amplitude, is 0.35 *m*. Local flow velocities of up to 1.2 *m/s* are observed [23]. In this paper, the month of October 2017 is simulated which contains both storm conditions and daily conditions. Observed water levels and wind velocities and directions within this period are displayed in (Figure 2). Relatively calm conditions occurred between days 9–22 and two storms occurred on days 5–6 and 28–29. During these storms, water levels reach up to 2.5 *m N.A.P.* and wind speeds reach 23 *m/s*. On average, based on local observations of the past 30 years, these water levels are exceeded 1.5 times annually [24]. The wind speeds are exceeded once per year [25]. Since two of these storms occur within the month of October 2017, our model setting could be classified as a rough simulation period.

Measurements of local bed material show median grain sizes ( $D_{50}$ ) ranging from 100–180  $\mu\text{m}$  [26] and 5–18% of the sediment consists of mud ( $p_m$ ) [23]. The salt marsh was growing during most of the 19th century after a groyne and sedimentation field were constructed. These sedimentation fields are a human intervention used to stimulate salt marsh growth. They consist of brushwood groynes (Figure 3c–e) which enclose areas of a marsh and tidal flat with the exception of small openings. This limits flow and wave energy within the area. Consequently, local sedimentation increases lead to marsh growth. However, after maintenance of these structures was halted, and the brushwood in

between the vertical poles started to wash away (Figure 3d), the salt marsh started to erode. Observed bed level changes between 2008 and 2014 are visualized (Figure 1d) [22]. The data exhibit an erosion rate of the salt marsh, the area with a bed level above 0.7 m N.A.P., of  $1.1 \text{ m}^3/\text{m}/\text{year}$  averaged along the marsh width. This erosion is mostly in the form of cliff erosion at the marsh front. The data additionally show a retreat rate of the marsh edge due to the cliff erosion of  $0.9 \text{ m}/\text{year}$  averaged along the marsh width.

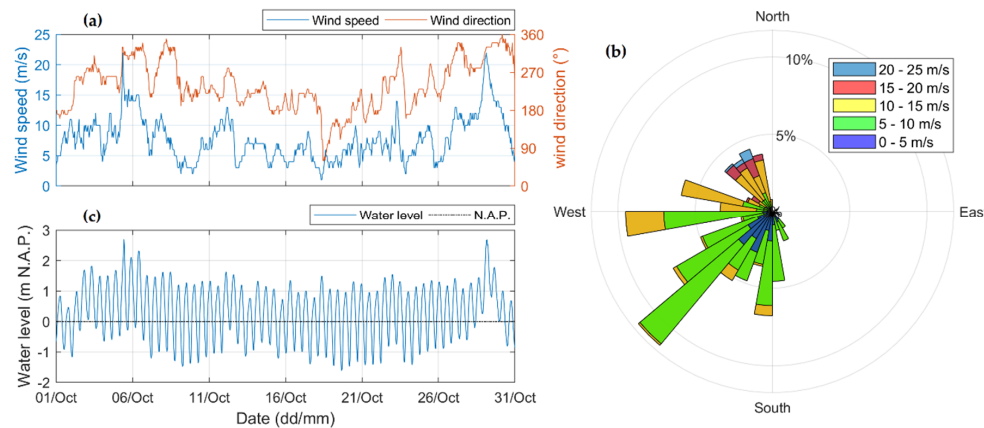


**Figure 2.** Observed hydrodynamic conditions during the simulated period nearby the study area. Displaying (a) wind velocities and directions at measurement station ‘Wierummerwad’ over time, (b) a wind rose of wind data at measurement station ‘Wierummerwad’, and (c) observed water level at measurement station ‘Lauwersoog’ over time. The time series show that two storms occur on days 5–6 and 28–29.



**Figure 3.** (a,b) Ground level view at the study site. The cliff height at the marsh front ranges from 0.2 to 1 m. (c) A degraded brushwood groyne where brushwood in between the vertical poles have washed away (Photo’s: R. Siemes). (d) A schematization of a traditional sedimentation field. Openings in between the brushwood groynes are to allow sediment supply. (e) A maintained brushwood groyne, part of a traditional sedimentation field [4] and (f) a conceptual visualization of artificial structures proposed by local authorities [27]. The figure displays a combination of a large groyne at the bottom right, and brushwood groynes.



## 2.2. Delft3D Flexible Mesh Description

A model is developed for the study area and its surroundings (Figure 1b). The purpose of the model is twofold. First, it is used (1) to study the processes that influence bed level change on an eroding marsh and, consequently, (2) to determine how configurations of artificial structures can be applied to improve hydrodynamic conditions and stimulate salt marsh growth.

A process-based numerical model was developed with Delft3D Flexible Mesh (v. 2019.2) in which both a flow and a wave module were applied. Within the flow module, the hydrodynamics are solved by using the 2D depth-averaged unsteady shallow-water equations. For the impact of wind on the flow module, the Charnock formulation was applied [28]. Within the wave module, waves are described based on the third-generation SWAN wave model, which considers wave propagation, wave breaking, diffraction, refraction, wind growth, and frequency shifting [29].

Sediment transport and bed level change is determined based on the formulation of Van Rijn (1993). The formulation distinguishes bed-load and suspended-load transport. Sediment advances through the flow based on a computed reference concentration. The method initially determines the magnitude of total bed-load transport, which is assumed to be comprised of two parts—current- and flow-related—which are subsequently computed based on total bed-load transport. Their directions are equal to the directions of the near-bed current and wave propagation, respectively [30]. For suspended sediment transport, the wave-related component is computed [31]. Based on the sediment transport, bed level change is determined. This is performed with source and sink terms where the erosive fluxes are due to the upward diffusivity of sediment and depositional fluxes are based on the settling of sediment.

To improve understanding of how the processes interact with each other, a diagram is made (Figure 4). A detailed model setup is available (Appendix A). Here, the model domain and timeframe and the setup of the hydrodynamics and sediment dynamics are mentioned. Input parameters are chosen which are typical for a Wadden Sea location. Table A1 shows an overview of these parameters (Appendix A).

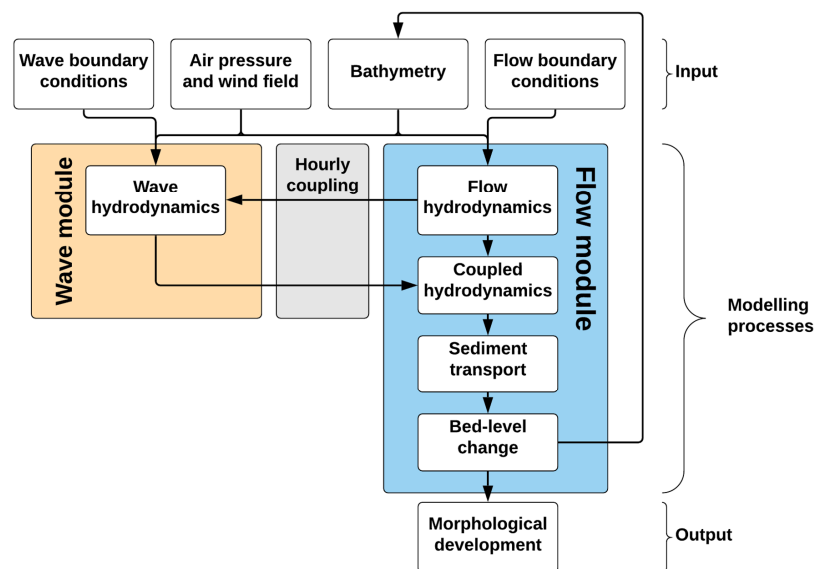


**Figure 4.** Schematization of processes introduced in Sections 2.2 and 2.3 and how these processes interact with each other in Delft3D Flexible Mesh. Arrows indicate the flow of data. The computational time step within the wave module is hourly. For the flow module, this is equal to the numerical time step. Arrows through the ‘hourly coupling’ section indicate the communication of data between the modules, which is performed hourly.

### 2.3. Addition of Artificial Structures

Artificial structures are geometrically implemented in the model to analyze their impact on the hydrodynamics and the morphological development. They are implemented in both the flow and wave modules, and they are represented as structures placed onto the model's grid lines. The structures affect the flow such that they simulate energy loss and redirect the flow. Within the wave module, the structures can attenuate waves with a transmission coefficient. This coefficient is either constant or it depends on the incident wave conditions, the height and shape of an artificial structure. Sediment transport, erosion, and deposition are only affected indirectly, due to the altered hydrodynamic conditions. Figure 5 visualizes the location of the various structures, and the specific structures implemented are described in brief in Table 1.

The structure named *Short* represents a small groyne of 2.5 m N.A.P. and reduces wave heights such that it represents a dam with a slope of 1:3/2 [32]. *Long* represents an extended version of *Short* with the same characteristics. These groynes represent the large groyne in Figure 3f.

Sedimentation fields are implemented in combination with the groynes. These sedimentation fields are constructed of brushwood groynes (Figure 3e) and have the specific purpose to reduce flow velocities and attenuate waves on, and in front of, a salt marsh to stimulate local sedimentation [33]. *Short + Traditional* is a combination of the short groyne and a sedimentation field with a traditional shape (Figure 3c,e) representing the structures present at the study area in the past. *Long + Alternative* is a combination of the long groyne with a configuration of an alternative sedimentation field proposed by local authorities (Figure 3f). This configuration is presumed to stimulate natural salt marsh morphology.

Within the flow module, the artificial structures applied for the sedimentation field have a height of 0.7 m above the initial bed level, with a maximum height of 1.45 m N.A.P. similar to sedimentation fields currently present in the Wadden Sea [33]. The same heights are applied for the implementation of *Short + Traditional* within the wave module, where the groynes represent a thin sheet. Wave attenuation for the sedimentation field of *Long + Alternative* is performed with a transmission coefficient of 0.55 [17]. It should be noted that, due to the resolution of the wave grid, the openings in between groynes of the sedimentation field are not present in the wave module. An overview of the specific input parameters applied for the various structures are available in Appendix B.

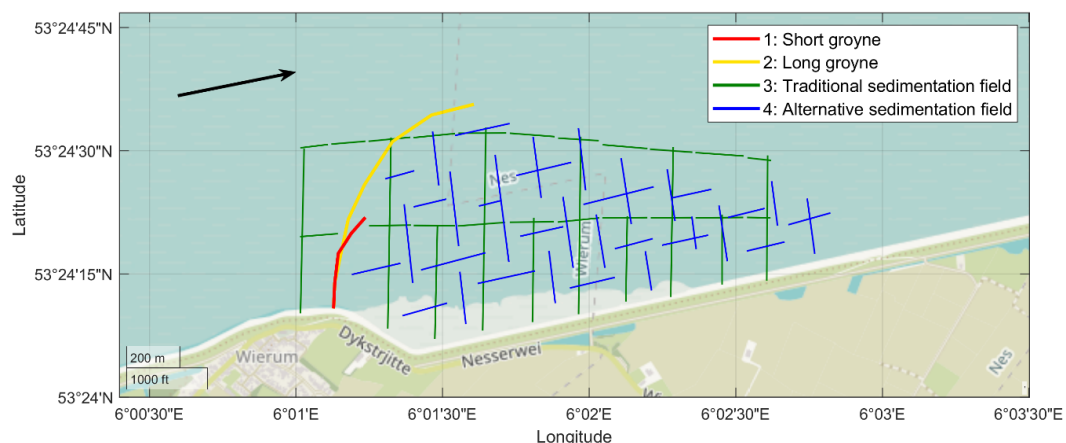


**Figure 5.** Visualization of the locations and shapes of the structures implemented within the model. The arrow indicates the dominant direction of tidal flow and alongshore transport.

**Table 1.** An overview of the artificial structure configurations.

Name	Structure Shape(s); as Referred to in Figure 5	Description
Short	1	A short groyne of 2.5 m high representing a structure such as large groyne in Figure 3f.
Long	2	A long groyne of 2.5 m high, similar as <i>Short</i> above.
Long + Alternative	2 + 4	Combination of <i>Long</i> and an alternative sedimentation field, representing a conceptual design (Figure 3f).
Short + Traditional	1 + 3	Combination of <i>Short</i> and a traditional sedimentation field. This configuration of sedimentation fields is often used in the past (Figure 3c).

### 3. Results

#### 3.1. Hydrodynamics

In order to improve simulation of the significant wave heights, calibration is performed for the bed friction coefficient of the wave module. This resulted in a Jonswap bed friction coefficient of  $0.058 \text{ m}^2 \text{ s}^{-3}$ . Subsequently, simulated water levels and the calibrated significant wave heights are validated at all measurement stations with available data. Results showed that the flow module performed well in simulating water levels (Figure 6). The wave module performed well for simulating wave heights (Figure 6). However, the highest wind waves are underestimated. Comparisons of observed and simulated data over time are shown in Appendix C.

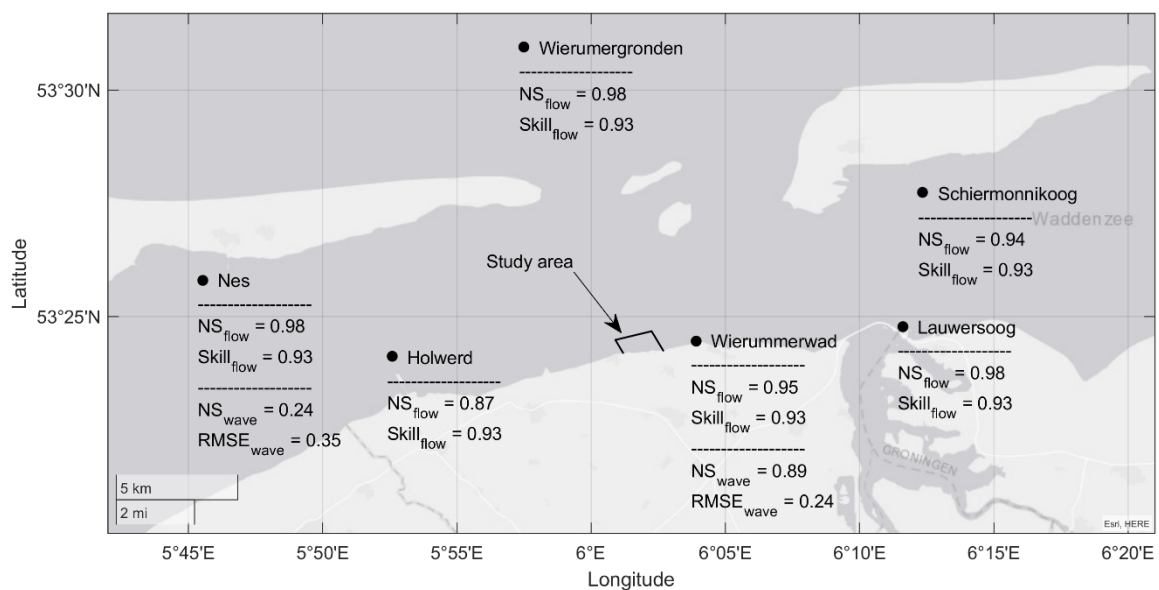


**Figure 6.** Validation of the hydrodynamics for all measurement stations within the model domain for which data are available. This is performed for the Nash Sutcliffe coefficient (NS) and index of agreement (Skill) for validation of the water levels in the flow module (flow). Similarly, it is performed for the NS and the root mean square error (RMSE) for the significant wave heights in the wave module (wave).

#### 3.2. Morphodynamics

##### 3.2.1. Salt Marsh Development without Human Interference

Based on these hydrodynamics, morphological development is simulated. The volumetric change over time within the study area is analyzed (Figure 7). Both the tidal flat and salt marsh show, when

inundated, erosion during ebb and accretion during flood. The figure also displays a dynamic tidal flat which undergoes both erosion and sedimentation. The salt marsh mostly displays a steady net erosion, almost entirely due to erosion of the marsh front.

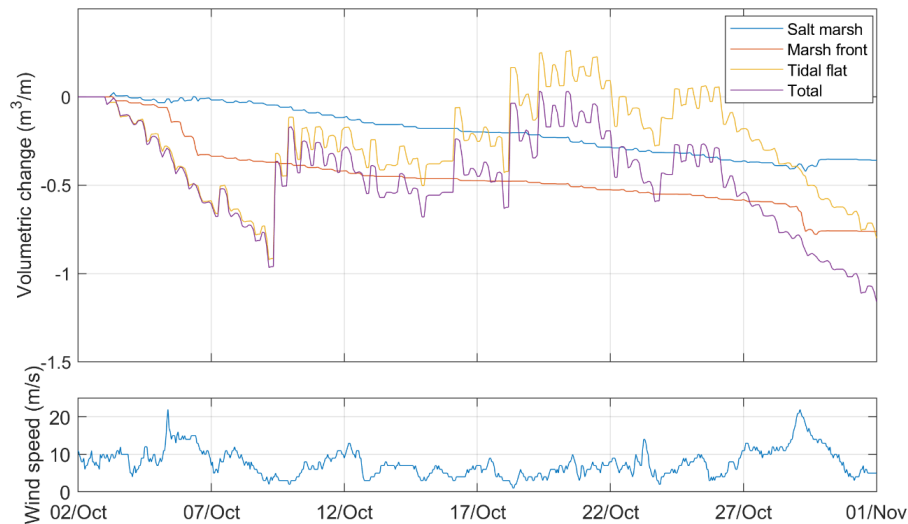


**Figure 7.** Simulated width averaged volumetric change ( $m^3/m$ ) over time within the study area (top) and the wind speeds during the simulation period (m/s) (bottom). The storms are during 4–5 October and 28–29 October. A relatively calm period is simulated from 9 to 22 October.

Results show that the tidal flat erodes during periods with heavy weather (Figure 7). However, in the middle of the simulated period, when conditions are calmer, the tidal flat exhibits net accretion for several tidal cycles. This accretion is strongest for the tidal cycles of 9 and 19 October. The part of the tidal flat close to the marsh undergoes net erosion, while areas with lower bed levels undergo net accretion (Figure 8).

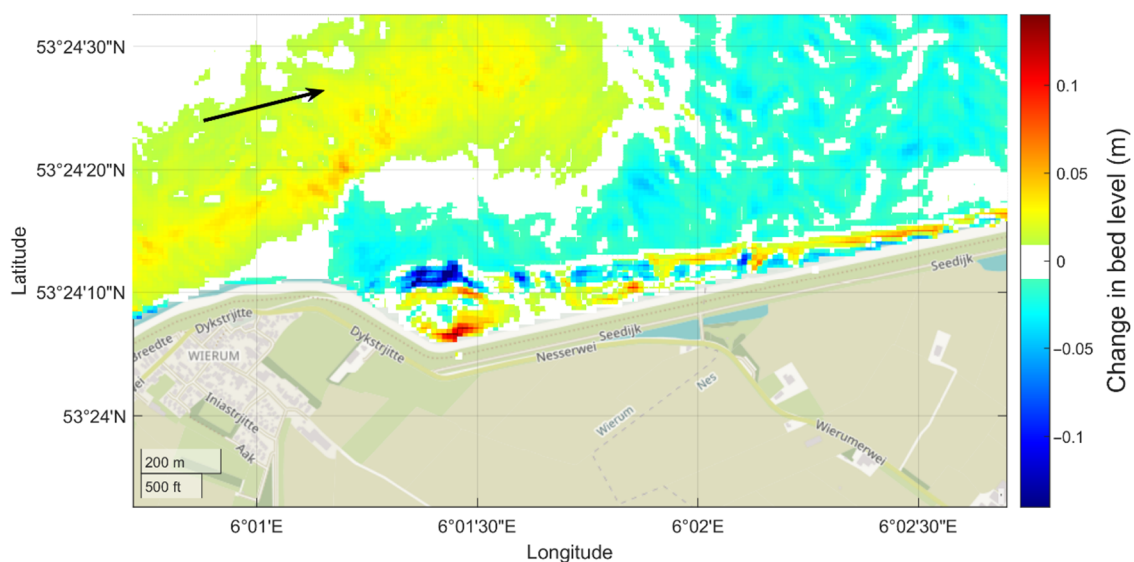


**Figure 8.** Total simulated bed level change (m) at the study area during October 2017. The arrow indicates the dominant direction of tidal flow and alongshore transport.

Furthermore, most of the erosion of the salt marsh can be observed along the marsh edge, representing cliff erosion. This erosion occurs along the first 25–50 m of the marsh front. The marsh front displays an increased erosion rate during storm periods (Figure 7). The figure also demonstrates



that total erosion of the marsh front is larger than the total salt marsh erosion, as accretion occurs on the marsh when inundated (Figure 8), which is mostly during storms. The total volumetric change on the salt marsh, modeled within the simulated month, is  $-0.36 \text{ m}^3/\text{m}$  (Figure 7).

### 3.2.2. Impact of Artificial Structures

Within the default simulation setting, the artificial structures are added. The structures named *Short* and *Long* cause set-up of the water level on the wind side and set-down on the lee side. Additionally, they attenuate waves and reduce flow velocities on their lee side. The short groyne shows little impact towards the hydrodynamics within the study area (Figure 9), since its area of effect is fairly small. The longer groyne affects a larger area and reduces waves and flow velocities to a larger degree. The groynes display a larger impact on the mean flow velocities during storms relative to calm weather, while the opposite is true for the mean wave heights.

Due to the changes in hydrodynamics caused by the groynes, morphological development is altered (Figure 9). The figure illustrates that both groynes reduce erosion of the marsh front. Accretion on the marsh is reduced as well. Erosion on the tidal flat directly in front of the marsh is reduced. However, the long groyne also causes net erosion further seawards. In addition, holes and depositional lobes develop at the tip of the groynes (Figure 10).

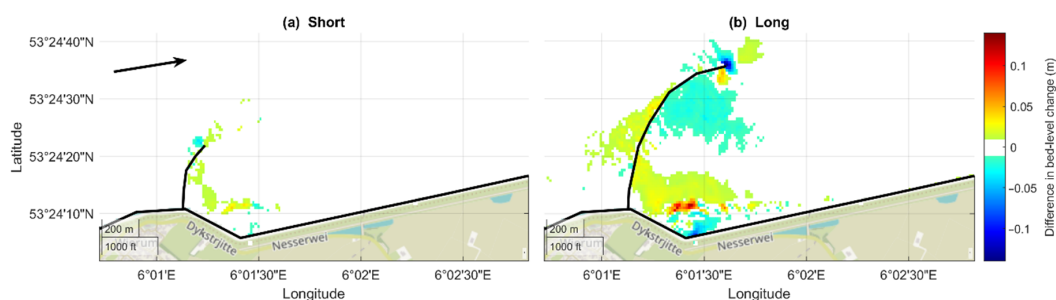


**Figure 9.** Difference in simulated bed level change compared to the default model for the structures (a) *Short* and (b) *Long*. Hard structures in the simulation are depicted by black lines. The arrow indicates the dominant direction of tidal flow and alongshore transport. The lee side is on the right of the structures.

For the scenario's *Long + Alternative* and *Short + Traditional*, sedimentation fields are added to the groynes. Due to the addition of the sedimentation fields to the long groyne (*Long + Alternative*), wave heights and flow velocities are further reduced (Table 2), further reducing erosion of the marsh edge and accretion on the marsh (Figure 11a,b). On the tidal flat, compared to the long groyne, the sedimentation field generally reduces local flow velocities during storms, while flow velocities remain similar during the calm period (Table 2). Consequently, net erosion on the tidal flat during storms is decreased, while net erosion during calm periods increases (Figure 11c).

**Table 2.** Comparison of hydrodynamics within the whole study area for the various configurations of artificial structures. Based on data with a two-hour interval. *Storm* refers to the average conditions during the storms of 4–5 October and 28–29 October. The *calm* period is from 9 to 22 October. *Total* is for the whole simulated month.

Simulation	Mean Flow Velocity (cm/s)			Mean Wave Height (cm)		
	Storm	Calm	Total	Storm	Calm	Total
Default	18.7	8.2	10.3	20.5	3.0	6.2
Short	17.5	7.9	9.9	19.9	2.8	5.9
Long	11.3	6.4	7.5	17.6	2.3	5.1
Long + Alternative	10.3	6.3	7.1	14.7	2.1	4.4
Short + Traditional	12.9	5.5	6.8	9.7	0.6	2.6

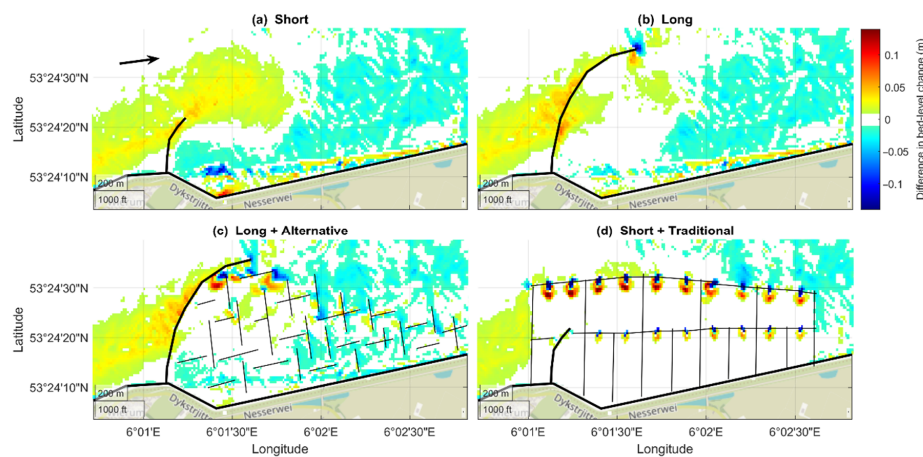


**Figure 10.** Simulated change in bed level within the study area for the structures (a) *Short*, (b) *Long*, (c) *Long + Alternative*, and (d) *Short + Traditional*. Hard structures in the simulation are depicted by black lines. The arrow indicates the dominant direction of tidal flow and alongshore transport. The lee side is on the right of the structures.

The artificial structures used for the scenario *Short + Traditional* display substantial impact for the whole study area. The sedimentation field reduces wave heights to a larger degree than for the scenario *Long + Alternative*. The structures *Short + Traditional* generate a constant attenuation of the flow velocity, both during calm weather and storms (Table 2). As a result, erosion on the tidal flat during storms is significantly reduced and sedimentation is observed during the calm period, resulting in net accretion for the whole simulated period (Figure 11c). On the tidal flat, in between the openings of the sedimentation fields, tidal channels are starting to form (Figure 10). The salt marsh itself undergoes almost no morphological development (Figure 11a).

Outside of the study area, all structures cause reduced erosion on the lee side. On the wind side, accretion is reduced. This effect is stretched out over 1 km along the coast on both sides and no differences larger than 1 cm are observed relative to the default simulation (Figure 9).

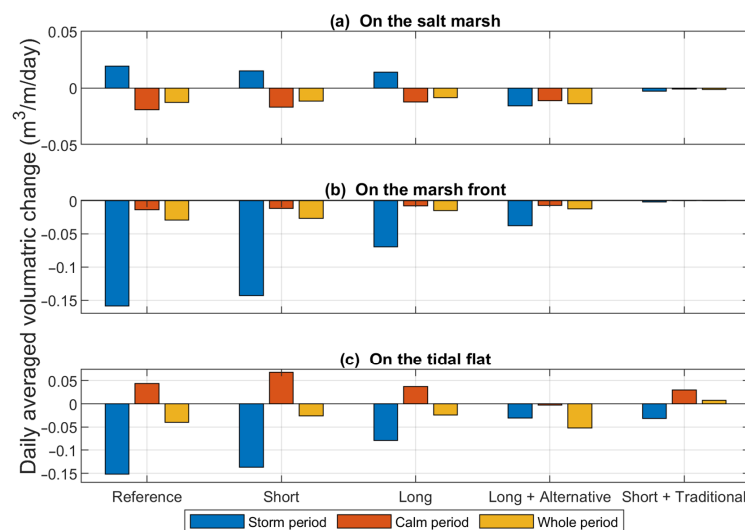


**Figure 11.** Daily and width averaged simulated volumetric change (a) on the salt marsh, (b) on the salt marsh front, and (c) on the tidal flat. The storm period is the combined bed level change during the storms of 4–5 October and 28–29 October. The calm period is from 9 to 22 October. The whole period is for the whole simulated month. “Reference” displays results of the simulation without artificial structures.

#### 4. Discussion

This paper reports on the first research application of the Delft3D Flexible Mesh modeling software in which a coupled flow-wave module and morphodynamics simulate salt marsh development. Both boundary and surface forcing are applied to successfully simulate daily and storm conditions. Based on the hydrodynamic forcing, bed level change on and around an eroding salt marsh is simulated. Due to the combination of boundary and surface forcing and by applying a flexible mesh, we are able to study both small- and large-scale morphological processes within the same simulation, while computation times can be kept relatively low (6 days on one computational core on a standard laptop). In addition, artificial structures are implemented in the model. These structures have shapes that represent structures used, or proposed, for marsh stimulation. The model provides the possibility to assess their impact on salt marsh dynamics within the study area.

##### 4.1. Assumptions and Uncertainties

To improve analysis and present results clearly, the area of interest is divided in three sections: the salt marsh, salt marsh front, and tidal flat (Figure 1c). While the boundaries for the salt marsh and salt marsh front are rather straightforward, the tidal flat is stated to end 1 km away from the coast, an assumption which is disputable. While altering the area of the tidal flat might change results quantitatively, qualitative results are expected to remain the same.

In addition, the model was run in 2DH, as solving the equations in 3D showed very similar results in comparative modeling studies [2,34] but it significantly increased computation time.

The model's sensitivity towards the wave height along the wave boundary ( $H_{s,BC}$ ) is assessed (Figure 12). This demonstrates that salt marsh development is not affected much by the  $H_{s,BC}$ . This indicates that wind waves within the study area, or more broadly within the Wadden Sea, depend almost entirely on the surface forcing within the simulation. This is also observed in practice by Oost [35]. Moreover, the limited model sensitivity towards the  $H_{s,BC}$  also shows that the method applied to estimate a wave boundary is sufficient for the purpose of this paper.

The surface forcing is simulated based on 'High Resolution Limited Area Model' (HiRLAM) data, which has a resolution of 11 by 11 km. Since the barrier islands of the Wadden Sea have similar dimensions, the impact of those islands on the wind velocities and directions are probably not considered well. Consequently, wave generation by wind on the lee side of the barrier islands may be overestimated. Nonetheless, wave heights are calibrated for local conditions, and the influence of overestimating wind velocities will thus be compensated for within the study area.

Within the flow module, vegetation is represented by using an increased bed roughness on the salt marsh. The impact of this bed roughness is included in the sensitivity analysis (Figure 12) where the model displays a high sensitivity towards the bed roughness on the marsh. The sensitivity analysis demonstrates that, due to an increase in bed roughness, marsh erosion is reduced. Vegetation is known to reduce marsh erosion [2]. Hence, this indicates that representing vegetation by an increased bed roughness achieves the anticipated effect of reduced marsh erosion. The ability of vegetation to function as sediment trap is not considered in the simulation, nor is the wave attenuating ability of the vegetation. However, salt marsh growth initiates with accretion of the tidal flat. Since vegetation is not likely to be present on the tidal flat within the simulated period, the simplified implementation of vegetation will not directly affect the analysis of salt marsh growth. However, it will reduce accretion and increase wave heights on the marsh itself.

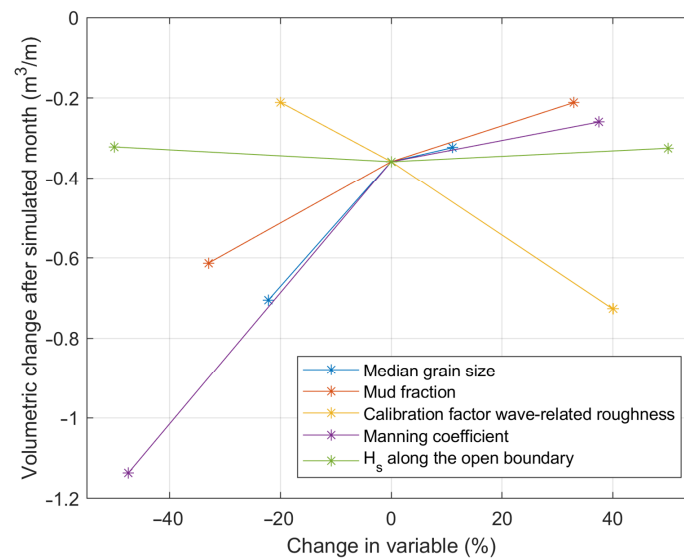


**Figure 12.** A sensitivity analysis with the width-averaged volumetric change of the salt marsh as indicator. The default case (0% change in variable) is the same simulation as in Section 3.2.1. The analysis is performed for the median grain size ( $D_{50}$ ), mud fraction ( $p_m$ ), calibration factor for wave-related roughness ( $R_{WAVE}$ ), Manning coefficient ( $n$ ), and significant wave height along the open boundary ( $H_{s,BC}$ ). Further information on the parameters is available in Appendix A (Table A1).

The sediment transport formulation of van Rijn (1993) is used to derive morphological development based on the hydrodynamic conditions. This formulation has reduced accuracy for bed material with  $D_{50} < 200 \mu m$ . In addition, the magnitude of sediment transport is sensitive towards wave-related bed-form roughness, an input parameter of which little data are available [31]. The wave-related bed-form roughness, as well as the  $D_{50}$  and  $p_m$ , input parameters of which no accurate data are available, are included in the sensitivity analysis (Figure 12). The model displays a high sensitivity towards these input parameters.

The applied sediment transport formulation is for non-cohesive sediments only. However, in reality, cohesive sediment is present as well [23]. The impact of cohesive sediment is simulated in a simplified manner, with a mud fraction. However, actual transport of cohesive sediment is not implemented, though this transport can lead to different morphological patterns [36]. Most notably, mud moves—to a larger extend than sand—to areas having lower energy such as a tidal flat and salt marsh [37]. The addition of mud transport is thus likely to result in increased sediment deposition in the higher regions of the study area.

Nonetheless, throughout the sensitivity analysis, differences in bed level change occurred mostly in the rate of erosion or accretion. Spatial morphological patterns remained similar throughout. Moreover, the simulation captures the governing processes for morphological development, such as accretion of the tidal flat and salt marsh during flood and erosion hereof during ebb. In addition, it displays a retreat of the marsh edge due to wave attacks, which increases with increasing wave heights (Figures 7 and 8), similar to what previous research indicated [11,12]. As observed by Oost [35], simulations show accretion on the marsh during storms as well (Figure 8). In addition, simulations display a stable marsh next to a dynamic tidal flat (Figure 7), as observed by Willemssen et al. [2]. This demonstrates the spatial robustness of the simulated morphological patterns. Similarly, Van der Wegen and Roelvink [38] also showed that model results do not change fundamentally when sediment characteristics are varied within a reasonable range.

#### 4.2. Default Simulation

Validation of the hydrodynamic conditions is performed for both the water levels and wave heights. While water levels are generally modeled well, differences are observed at low water levels at



some measurement stations. This is caused by differences in bed level, since the local bathymetry data originate from 2012 while the model simulates a period in 2017. The significant wave heights were simulated reasonably well. However, low wave heights were underestimated, which is most likely also caused by the differences in bed level. High waves are underestimated as well, which may be caused by a wave-breaking parameter which is too low (Appendix C).

Validation of the simulated morphological development is performed by a comparison with the observed long-term morphological development. Besides that, several morphological processes are identified in literature as well. For instance, results indicate that almost all morphological development on the tidal flat and salt marsh occur due to wind waves. This is supported by literature, which indicates that wind waves are directly related to both sediment supply and erosion rates for salt marshes [11,20]. In addition, both the tidal flat and salt marsh show, when inundated, erosion during ebb and accretion during flood (Figure 7). This is supported by basic theory on salt marsh evolution [39]. Results also demonstrate a dynamic tidal flat next to a relatively stable marsh (Figure 7), which is observed by Willemsen et al. [2]. At the marsh front, an increased erosion rate is observed during storm periods, when waves are higher, which is supported by theory on salt marsh cliff erosion [11]. During these storms, accretion on the salt marsh is observed. This process is identified in literature as well, where Oost [35] reports up to several decimeters of accretion after a storm.

Observed bed level data exhibited annual volumetric change averaged along the width of the salt marsh of  $-1.1 \text{ m}^3/\text{m}/\text{year}$  (Figure 1d). Applying the same method of data analysis for the simulation exhibits a volumetric change of  $-0.36 \text{ m}^3/\text{m}/\text{month}$  (Figure 7). Morphological development of a marsh mainly occurs within the period of October till February [35]. Assuming all bed level change on a marsh occurs within these 5 months, and erosion during those months is equal, results in an estimated simulated erosion of  $1.8 \text{ m}^3/\text{m}/\text{year}$ . This is an overestimation of 64%. One could argue that two storms are present within the simulated month, with water levels and wind speeds which have a reoccurrence frequency of 1.5 times [24] and 1 time per year [25], respectively. Consequently, erosion rates within the simulated month will be higher. However, during the storms, slight net accretion is simulated on the salt marsh (Figure 7), refuting this argument. While storms do not increase net erosion of the marsh, the storms do increase erosion of the salt marsh front. Therefore, large erosion rates are simulated here.

Salt marsh growth is initiated by accretion of the tidal flat. The observed bed level data already shows accretion of the tidal flat (Figure 1d), which suggests that the study area has potential for salt marsh growth. In the simulation, that same area shows net erosion (Figure 8). The cause hereof is the heavy weather that is simulated, since accretion is simulated during relatively calm weather (Figure 7), indicating that the potential for marsh growth is present in the simulation as well.

The simulated erosion along the marsh front occurs due to wave energy, similar to realistic erosion of a marsh cliff [12]. However, the model does not simulate a retreating marsh due to actual cliff erosion as displayed in the observed data (Figure 1d). Hence, simulated erosion of the marsh occurs along 25–50 m of the marsh front's length (Figure 8). The cause of this limitation is that the processes required to accurately describe cliff erosion are not part of D3D-FM [40]. In addition, due to the absence of a marsh cover with increased cohesiveness and vegetation, the marsh front will undergo additional erosion [41]. These limitations should be considered when interpreting the results.

#### 4.3. Artificial Structures

The results with artificial structures indicate that, while the groynes are able to reduce energy within the study area, sedimentation fields show larger potential to steer morphological development of the marsh and tidal flat. Not only do the sedimentation fields depend less on the wind direction to effectively attenuate waves, they are also able to consistently and considerably reduce flow velocities (Table 2).

The groynes do display the ability to stimulate salt marsh growth by reducing wave heights and flow velocities. Consequently, local bed shear stresses and thus erosion rates are reduced. In addition, sediment in the water column has more time to settle due to reduced flow velocities [40]. However,

several processes limit their potential. During the simulated storms, waves come from a northern direction, limiting their area of effect and thus their effectiveness. In addition, *Long* causes increased net erosion on parts of the tidal flat (Figure 9) which is caused by the structure blocking alongshore sediment transport, limiting sediment supply. This process affects the configurations with sedimentation fields as well.

The potential of sedimentation fields to stimulate salt marsh development is most notably in *Short + Traditional*. Both flow velocities and wave heights are substantially reduced due to the addition of the sedimentation field to the short groyne (Table 2). As a consequence hereof, erosion is minimal during the entire simulated period (Figure 11). In addition, on the tidal flat, *Short + Traditional* is the only configuration which results in net accretion for the whole period (Figure 11).

In *Long + Alternative*, the addition of a sedimentation field to the long groyne does not reduce flow velocities and wave heights to such an extent as the traditional sedimentation field of *Short + Traditional* does (Table 2). Moreover, the impact of *Long + Alternative* on bed level change is not as substantial as for *Short + Traditional* (Figure 11), though the structures implemented for these sedimentation fields have a similar total length. This indicates that, while sedimentation fields can have a large impact, a proper configuration of the structure should be implemented to be efficient and effective.

Four different morphological developments of salt marshes or tidal flats are identified which are likely the crucial indicators for policy makers when steering salt marsh development (Table 3). The artificial structures are ranked on how well they performed in impacting these specific morphological developments. Accretion of the marsh and erosion of the marsh front display a negative relationship. Namely, wave attenuation results in reduced erosion of the marsh front. However, less sediment is transported onto the marsh as well, reducing marsh accretion. To assess which structure performs best to stimulate salt marsh growth, there are two indicators. When a tidal flat is not sufficiently high—relative to the water level—for vegetation to establish, accretion of the tidal flat is the crucial indicator. When a tidal flat has sufficiently accreted for vegetation establishment, the stability of the tidal flat is of key importance, since large perturbation of the bed level will cause burying or toppling of pioneer vegetation [13,15].

**Table 3.** Qualitative ranking of how well the artificial structures can steer specific morphological development.

Structure Name	Short	Long	Long + Alternative	Short + Traditional
Allowing accretion salt marsh	1	2	3	4
Reduced erosion marsh front	4	3	2	1
Accretion tidal flat	3	2	4	1
Stability tidal flat	4	3	2	1

It should be considered that the impact of structures is assessed for an eroding marsh. When a salt marsh is healthy, and no cliff erosion occurs, the same analysis may provide different results. In addition, although the results show clear erosion and accretion trends, only the initial impact after structure implementation is simulated. The impact of the structures and of initial bed level changes on long-term morphological development is left for further study. Similarly, outside of the study area, little differences in bed level change were observed due to the structures. However, this may be different when a longer period is simulated. Furthermore, permeable structures could not be implemented within the model. Since results indicate that the restriction of flow has both pros and cons, by reducing flow velocities but blocking alongshore sediment transport as well, permeable groynes may prove to an effective tool for steering salt marsh development.

In this paper, we looked at four structure configurations. For future work, a larger range of structures can be studied. Such research can be particularly useful to optimize the design of a structure. Hereby, optimization should not only focus on stimulating salt marsh growth, but also take into account the interest of the various stakeholders, such as Natura2000 or local authorities.

#### 4.4. General Applicability

Within this paper, morphological development of a salt marsh is simulated. The methods used to set up the model can be applied to create a similar model focusing on other salt marshes. This can be within the Wadden Sea, or more widely, within the area encompassed within the DCSM-FM model, since the used surface forcing from the HiRLAM dataset covers this area as well. The model setup can be adapted such that it can be used for long-term modeling as well. However, the simplified implementation of vegetation will probably not suffice since vegetation establishment is not being explicitly accounted for [13,15]

Results show that there is potential for salt marsh growth within the study area. Not only does the tidal flat already show slight accretion (Figure 1d), the implemented structures, and most notably *Short + Traditional*, are able to reduce salt marsh erosion and stimulate its growth by increasing accretion on the tidal flat (Figure 11).

More broadly, the simulations show that the salt marsh accretes during storm events (Figure 11). This demonstrates that salt marsh systems may provide a resilient supplement to hard structures to improve coastal safety in the face of the increasing storminess [42].

Moreover, results with artificial structures indicate that morphological development of a salt marsh can be steered by implementing various structures. Groynes can reduce erosion rates of the marsh front and are able to increase accretion of the tidal flat during calm weather. However, their potential impact on morphological development is not as substantial as sedimentation fields. The sedimentation fields, and most notably the traditional configuration, have the potential to further reduce marsh erosion and cause accretion on the tidal flat in front of the entire salt marsh, proving to be a viable tool for stimulating salt marsh growth.

## 5. Conclusions

This paper shows how artificial structures can be used to steer the morphological development of salt marshes. This is performed with a morphological model (Delft3D-FM) which is set up for an eroding marsh. Daily conditions and two storms with a reoccurrence of 1–1.5 times annually are simulated. Additionally, artificial structures with shapes representing reality are implemented to analyze how they affect morphological development.

Our results show that the governing processes for morphological development of salt marshes are well captured within the simulations. Simulations show potential for artificial structures to reduce erosion and stimulate salt marsh growth. Most notably, traditional sedimentation fields perform substantially better than the other configurations. This structure minimalizes erosion and generates sufficiently calm conditions for sediment to settle.

It should be considered that the simulation demonstrates how the study area is affected directly after structure implementation (1 month). However, morphological processes often occur on a time scale of years or decades. In addition, processes related to cliff erosion are not accounted for. Future research on development of the marsh cliff and on the impact of various structures on long-term morphological development is advised.

**Author Contributions:** R.W.A.S. constructed the model, designed the model experiments, prepared the figures and wrote most of the text; B.W.B. promoted the research and reached out to stakeholders and authorities to exchange information and data; R.J.D. guided model building and aided with troubleshooting with the software which was under development; S.J.M.H.H. supervised the research; Manuscript conception is performed by R.W.A.S., B.W.B., and S.J.M.H.H.; B.W.B., R.J.D. and S.J.M.H.H. provided intellectual input, edited the manuscript and performed proofreading. All authors have read and agreed to the published version of the manuscript.

**Funding:** This research received no external funding.

**Acknowledgments:** The authors would like to acknowledge the reviewers and editor for their helpful suggestions and comments. Also, we would like to thank Harry Feenstra and Bram Hulsman for their active involvement and for sharing their knowledge of the study area.

**Conflicts of Interest:** The authors declare no conflict of interest.

## Appendix A. Model Setup

### Appendix A.1. Domain and Timeframe

The model consists of separate domains for the wave and flow modules. The flow domain includes an area of 80 by 50 km in which the study area is centered. At the outer edge of the domain, the resolution is 800 by 800 m and the grid is refined in four steps towards the study area. The first and fourth refinement steps are with a factor 4 and the second and third with a factor 2, for a total refinement of factor 64. This results in a grid size of 12.5 by 12.5 m within the area of interest, which is 5 by 2 km. The grid is made up of mostly squares, with triangles along the refinements. Within the wave module, a curvilinear grid is applied. The grid has a resolution of 2 by 3 km at the northern edges which reduces towards the study area where grid sizes are 150 by 150 m. The domain areas and their main characteristics are visualized in Figure 1b. In both domains diked areas, including the dikes themselves, are flow and wave restricted.

The area encompassed by the outer refinement step of the flow domain has bathymetry data obtained from the publicly available Open Earth dataset [43]. Bathymetric data for the remaining domain area originate from the Netherlands Hydrographic Office [44]. Within the flow domain, a spatially varying Manning coefficient is used for the bed-roughness. Most of the domain has a Manning coefficient of  $0.021 \text{ s m}^{-1/3}$ , as derived by Zijl et al. [45]. However, on the salt marsh, vegetation is present in the form of a grassy top which increases the bed-roughness. This vegetation is represented with a manning coefficient of  $0.04 \text{ s m}^{-1/3}$  [46]. The bed-roughness applied within the wave module is determined through calibration (discussed in Appendix A.3).

Furthermore, eddy viscosity and diffusivity are implemented for the flow module's turbulence model. The horizontal eddy viscosity varies throughout the domain based on the local grid size [32,47] which is performed by applying a Smagorinsky factor with a typical value of 0.15 [48]. Based on this factor, a local horizontal eddy viscosity is derived. For the horizontal eddy diffusivity, a value of  $1 \text{ m}^2/\text{s}$  is implemented which is suitable for the grid size in and around the area of interest [32].

Two different time steps are applied. While the wave module computes wave conditions with an hourly interval, the flow module applies a numerical time step which is based on a maximum Courant number of 0.7. This time step is also applied for morphological computations. Communication between the modules is performed hourly. An appropriate hydrological spin-up period of two days is used, which is necessary for the currents to adapt to the water level forcing.

**Table A1.** Overview of the applied input parameters.

Parameter	Value	Definition	Source
Domain and time frame			
$n$	$0.021 \text{ s m}^{-1/3}$	Manning coefficient	[45]
$n_{\text{marsh}}$	$0.04 \text{ s m}^{-1/3}$	Manning coefficient on the salt marsh	[46]
$C_{\text{bottom}}$	$0.058 \text{ m}^2 \text{ s}^{-3}$	Jonswap bed friction coefficient	i
$C_S$	0.15	Smagorinsky factor	[48]
$K$	$1 \text{ m}^2 \text{ s}^{-1}$	Horizontal eddy diffusivity	[47]
$C_{\text{max}}$	0.7	Maximum courant number	[32]
Sediment dynamics			
$\rho_{\text{sed}}$	$2650 \text{ kg m}^{-3}$	Specific sediment density	[32]
$P_{\text{bed}}$	$1600 \text{ kg m}^{-3}$	Dry bed density	[32]
$D_{50}$	$180 \mu\text{m}$	Median grain size	ii
$p_m$	0.15 (-)	Mud fraction	ii
RWAVE	1.25 (-)	Calibration factor for wave-related bed-form roughness	ii

<sup>i</sup> Determined based on calibration of hydrodynamics. <sup>ii</sup> Determined based on initial model testing, performed to improve simulated morphological development (Appendix A.3).



### Appendix A.2. Hydrodynamics

To derive boundary conditions for the flow module, the Dutch continental shelf model is used (DCSM-FM Model). The DCSM-FM model was developed in-house at Deltares and is able to simulate the effect of tides and storm surges. At the open boundary of the DCSM-FM model, a forcing of the water level is implied using astronomical components. These astronomical components are derived from the tidal model, FES2012 [49]. Furthermore, meteorological surface forcing is included, which enables the simulation of storm surging. This is performed by adding time- and space-varying wind velocities and air pressure. From this DCSM-FM model, water levels and flow velocities vectors are extracted with a time step of five minutes along the open boundary of the flow domain.

Input for the wave module's boundary condition is estimated, since insufficient data are available along this boundary. The wave heights are estimated based on measured wave heights at the 'Eierlandse Gat boei' [24] and expected wave heights based on observed wind velocities according to Wright et al. [50]. This results in wave heights along the boundary between 0.5 to 9 m occurring with wind velocities between 1 to 23 m/s. Wave periods are based on the relation between wave height and period [51]. Furthermore, the wave direction is assumed to be equivalent to the wind direction. Since all this data is hourly, the wave-boundary condition has hourly data as well.

Due to the dimensions of both domains, surface forcing is required. For this purpose, data from the 'High Resolution Limited-Area Model' (HiRLAM) are applied, which contain hourly wind vectors and air pressure data with a resolution of 11 by 11 km [52]. For both the flow and wave modules, wind data are applied, which accommodates both the wind velocity and direction. Within the flow module, air-pressure data are used as well.

Research indicates that wind waves are an important factor for salt marsh development, both for accretion by sediment supply and for erosion by wave action [12,19]. Therefore, optimization of wind wave modeling is desirable. This will be performed by calibrating the bed friction coefficient within the wave module for both the Jonswap and Madsen formulation [53,54].

At measurement station 'Wierummerwad' (see Figure 6 for measurement location), which is nearest to the area of interest, observed and measured wave heights will be compared to identify the optimal bed friction coefficient. The optimum will be determined based on the Nash Sutcliffe coefficient (NS) [55]. This coefficient is chosen because high values have a comparatively higher impact, which is also true for erosion by wind waves [11].

In addition, the simulated hydrodynamics will be validated by comparing the output with observed historical water levels at all available measurement stations within the model domain. For validation of the water levels, this will be performed using the 'index of agreement' (Skill) focusing on mean values [56,57] and with the NS, which focuses on extremes [55]. The data will be compared with a five-minute interval. Validation at the location nearest to the area of interest is performed for November 2017 due to data availability. The wave module will be validated similarly, based on the wave heights. This will be performed with the NS and the root mean square error (RMSE). This comparison will be based on hourly data.

### Appendix A.3. Sediment Dynamics

Within the model, the bed consists of uniform and homogeneous sand with a single median grain size. The specific and dry-bed density are  $2650 \text{ kg/m}^3$  and  $1600 \text{ kg/m}^3$ , respectively, which are in agreement with literature [58]. For the sediment-transport formulation of Van Rijn [30], default D3D-FM settings were used [40]. Additionally, a Neumann boundary condition is set for the sediment transport. With this option, flow entering the system carries sediment at equilibrium concentration profiles. This effectively limits bed level change at the open boundaries.

The sediment transport formulation is for non-cohesive sediments, though in reality, cohesive sediment is also present within the Wadden Sea [23,26]. When an increasing fraction of mud is present in the sediment, the bed gradually approaches a cohesive regime, which leads to altered erosion

patterns [36]. To simulate the presence of cohesive sediment, a mud fraction ( $p_m$ ) is used. This is implemented such that:

$$\tau_{e,cr} = \tau_{s,cr}(1 + p_m)^\beta, \quad (A1)$$

where  $\tau_{e,cr}$  is the critical bed shear stress for erosion (Pa),  $\tau_{s,cr}$  is the critical bed shear stress for sand (Pa),  $p_m$  is the mud fraction (-), and  $\beta$  is the empirical constant for critical bed shear stress for erosion (-), which is 3 [59].

To improve the simulated salt marsh erosion rate, initial model testing is performed. This was performed in comparison to the observed annual erosion rate of the marsh (Section 2.1). Based on this initial model testing, a  $D_{50}$  of 180  $\mu\text{m}$  and a  $p_m$  of 0.15 are determined. These values are within the bandwidth in which they are observed nearby the study area as identified by Deltares [26] and Zwarts et al. [23], respectively. Similarly, the wave-related roughness is lowered from its default setting which is performed by setting the calibration factor hereof ( $RWAVE$ ) at 1.25, which is within the advised range for this calibration factor of 1–3 [40].

The morphological development simulated with the above-mentioned settings is validated. Unfortunately, repeated bathymetric data measurements are scarce worldwide, and also unavailable within the model domain. Consequently, bed level change is validated qualitatively using the observed long-term bed level data (6-year interval; Section 2.1) and literature on the morphological evolution of salt marshes.

## Appendix B. Input Parameters Structure Implementation

**Table A2.** Input parameters applied for the implementation of artificial structures.

Parameter	Value	Definition	Module	Source
<b>Short; Long</b>				
$H$	2.5 m	Height structure	Flow	<sup>i</sup>
$H_D$	2.5 m	Dam height	Wave	<sup>i</sup>
$\alpha_D$	2.6 (-)	Alpha of dam	Wave	[32]
$B_D$	0.15 (-)	Beta of dam	Wave	[32]
<b>Long + Alternative</b>				
$H$	Max 0.75 m above bed level -or- 1.45 m N.A.P.	Height structure	Flow	[33]
$K_{bg}$	0.55 (-)	Transmission coefficient of brushwood groyne	Wave	[17]
<b>Short + Traditional</b>				
$H$	Max 0.75 m above bed level -or- 1.45 m N.A.P.	Height structure	Flow	[33]
$\alpha_G$	1.8 (-)	Alpha of brushwood groyne	Wave	[32]
$B_G$	0.10 (-)	Beta of brushwood groyne	Wave	[32]

<sup>i</sup> Equal to other groynes in the Wadden Sea [22].

## Appendix C. Comparison Hydrodynamics

### Appendix C.1. Flow Module

The observed and modeled water levels at measurement station ‘Lauwersoog’ are compared (Figure A1). The figure displays that the model performs well for both the extreme and mean water levels.

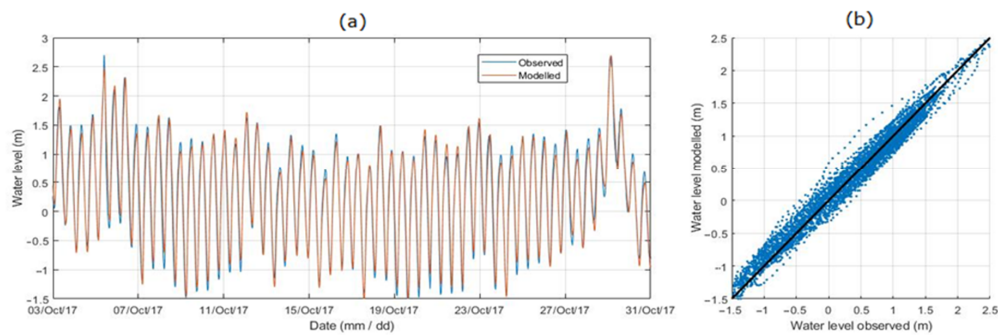


**Figure A1.** Comparison of observed and modeled water levels at measurement station 'Lauwersoog' (a) over time and (b) in a scatter plot with identity line (black solid line).

### Appendix C.2. Wave Module

The wave module is calibrated on the significant wave height. The calibration, with an optimization for the NS, resulted in a Jonswap bed friction coefficient of  $0.058 \text{ m}^2 \text{ s}^{-3}$ . A comparison of the wave heights for an advised Jonswap bed friction coefficient of  $0.038 \text{ m}^2 \text{ s}^{-3}$  [60] and the optimal value is displayed for the measurement station 'Wierummerwad' (Figure A2). Although the peak wave height is simulated less accurately with the optimized bed friction, the model exhibits improved performance for most wave heights, thereby resulting in an improved NS.

The model performs well for the measurement station 'Wierummerwad'. In general, it underestimates extreme values, and mid-range values are overestimated. At measurement station 'Nes', the high waves are simulated worse compared to station 'Wierummerwad', while low- and mid-range values are modeled similarly.

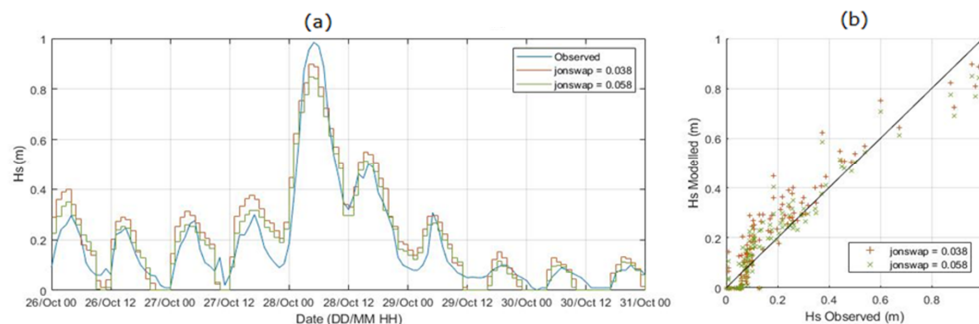


**Figure A2.** Comparison of observed and modeled significant wave heights with the advised and calibrated bed friction at measurement station 'Wierummerwad' (a) over time and (b) in a scatter plot with an identity line (black solid line).

### References

1. Vuik, V.; Jonkman, S.N.; Borsje, B.W.; Suzuki, T. Nature-based flood protection: The efficiency of vegetated foreshores for reducing wave loads on coastal dikes. *Coast. Eng.* **2016**, *116*, 42–56. [\[CrossRef\]](#)
2. Willemsen, P.W.J.M.; Borsje, B.W.; Hulscher, S.J.M.H.; van der Wal, D.; Zhu, Z.; Oteman, B.; Evans, B.; Moller, I.; Bouma, T.J. Quantifying Bed Level Change at the Transition of Tidal Flat and Salt Marsh: Can We Understand the Lateral Location of the Marsh Edge? *J. Geophys. Res. Earth Surf.* **2018**, *123*, 2509–2524. [\[CrossRef\]](#)
3. Kirwan, M.L.; Temmerman, S.; Skeehean, E.E.; Guntenspergen, G.R.; Fagherazzi, S. Overestimation of marsh vulnerability to sea level rise. *Nat. Clim. Chang.* **2016**, *6*, 253–260. [\[CrossRef\]](#)
4. Vuik, V.; Borsje, B.W.; Willemsen, P.W.; Jonkman, S.N. Salt marshes for flood risk reduction: Quantifying long-term effectiveness and life-cycle costs. *Ocean Coast. Manag.* **2019**, *171*, 96–110. [\[CrossRef\]](#)

5. Wanner, A.; Suchrow, S.; Kiehl, K.; Meyer, W.; Pohlmann, N.; Stock, M.; Jensen, K. Scale matters: Impact of management regime on plant species richness and vegetation type diversity in Wadden Sea salt marshes. *Agric. Ecosyst. Environ.* **2014**, *182*, 69–79. [[CrossRef](#)]
6. Chmura, G.L.; Anisfeld, S.C.; Cahoon, D.R.; Lynch, J.C. Global carbon sequestration in tidal, saline wetland soils. *Glob. Biogeochem. Cycles* **2003**, *17*. [[CrossRef](#)]
7. Jones, M.B.; Donnelly, A. Carbon sequestration in temperate grassland ecosystems and the influence of management, climate and elevated CO<sub>2</sub>. *New Phytol.* **2004**, *164*, 423–439. [[CrossRef](#)]
8. Costanza, R.; d'Arge, R.; De Groot, R.; Farber, S.; Grasso, M.; Hannon, B.; Limburg, K.; Naeem, S.; O'Neill, R.V.; Paruelo, J.; et al. The value of the world's ecosystem services and natural capital. *Nature* **1997**, *387*, 253–260. [[CrossRef](#)]
9. Millard, K.; Redden, A.M.; Webster, T.; Stewart, H. Use of GIS and high resolution LiDAR in salt marsh restoration site suitability assessments in the upper Bay of Fundy, Canada. *Wetl. Ecol. Manag.* **2013**, *21*, 243–262. [[CrossRef](#)]
10. Chang, E.R.; Veeneklaas, R.M.; Bakker, J.P.; Daniels, P.; Esselink, P. What factors determined restoration success of a salt marsh ten years after de-embankment? *Appl. Veg. Sci.* **2016**, *19*, 66–77. [[CrossRef](#)]
11. Leonardi, N.; Ganju, N.K.; Fagherazzi, S. A linear relationship between wave power and erosion determines salt-marsh resilience to violent storms and hurricanes. *Proc. Natl. Acad. Sci.* **2016**, *113*, 64–68. [[CrossRef](#)] [[PubMed](#)]
12. Bouma, T.J.; Van Belzen, J.; Balke, T.; Van Dalen, J.; Klaassen, P.; Hartog, A.M.; Callaghan, D.P.; Hu, Z.; Stive, M.J.; Temmerman, S.; et al. Short-term mudflat dynamics drive long-term cyclic salt marsh dynamics. *Limnol. Oceanogr.* **2016**, *61*, 2261–2275. [[CrossRef](#)]
13. Hu, Z.; van Belzen, J.; van der Wal, D.; Balke, T.; Wang, Z.B.; Stive, M.; Bouma, T.J. Windows of opportunity for salt marsh vegetation establishment on bare tidal flats: The importance of temporal and spatial variability in hydrodynamic forcing. *J. Geophys. Res. Biogeosci.* **2015**, *120*, 1450–1469. [[CrossRef](#)]
14. Silinski, A.; Fransen, E.; Bouma, T.J.; Meire, P.; Temmerman, S. Unravelling the controls of lateral expansion and elevation change of pioneer tidal marshes. *Geomorphology* **2016**, *274*, 106–115. [[CrossRef](#)]
15. Poppema, D.W.; Willemsen, P.W.; de Vries, M.B.; Zhu, Z.; Borsje, B.W.; Hulscher, S.J. Experiment-supported modelling of salt marsh establishment. *Ocean Coast. Manag.* **2019**, *168*, 238–250. [[CrossRef](#)]
16. Van Loon-Steensma, J.M.; Slim, P.A. The impact of erosion protection by stone dams on salt-marsh vegetation on two Wadden Sea barrier islands. *J. Coast. Res.* **2012**, *29*, 783–796. [[CrossRef](#)]
17. Dao, T.; Stive, M.J.; Hofland, B.; Mai, T. Wave Damping due to Wooden Fences along Mangrove Coasts. *J. Coast. Res.* **2018**, *34*, 1317–1327.
18. Vona, I.; Gray, M.W.; Nardin, W. The Impact of Submerged Breakwaters on Sediment Distribution along Marsh Boundaries. *Water* **2020**, *12*, 1016. [[CrossRef](#)]
19. Schuerch, M.; Spencer, T.; Evans, B. Coupling between tidal mudflats and salt marshes affects marsh morphology. *Mar. Geol.* **2019**, *412*, 95–106. [[CrossRef](#)]
20. Best, U.S.N.; van der Wegen, M.; Dijkstra, J.; Willemsen, P.W.J.M.; Borsje, B.W.; Roelvink, D.J.A. Do salt marshes survive sea level rise? Modelling wave action, morphodynamics and vegetation dynamics. *Environ. Model. Softw.* **2018**, *109*, 152–166. [[CrossRef](#)]
21. Loon-Steensma, J.M.; Groot, A.V.; Duin, W.E.; Wesenbeeck, B.K.; Smale, A.J. *Zoekkaart Kwelders en Waterveiligheid Waddengebied*; Alterra-rapport 2391; Alterra: Wageningen, The Netherlands, 2012.
22. RWS (Ed.) Actueel Hoogtebestand Nederland (AHN). 2014. Available online: [AHN.nl](https://ahn.nl) (accessed on 6 May 2019).
23. Zwarts, L.; Dubbeldam, W.; van den Heuvel, H.; van de Laar, E.; Menke, U.; Hazelhoff, L.; Smit, C. *Bodemgesteldheid en Mechanische Kokkelvisserij in de Waddenzee*; RIZA Rapport; RIZA: Lelystad, The Netherlands, 2004.
24. RWS (Ed.) Water-Info. 2019. Available online: [Waterinfo.rws.nl](https://waterinfo.rws.nl) (accessed on 6 May 2019).
25. K.N.M. Instituut. Klimatologie. Hourly Weather Data in the Netherlands. 2019. Available online: <https://projects.knmi.nl/klimatologie/uurgegevens/selectie.cgi> (accessed on 6 May 2019).
26. Deltares. Dataset: Sediment. Atlas Wadden Sea. RWS, Ed.; 2015. Available online: [publicwiki.deltares.nl/display/OET/Dataset+documentation+Sediment+atlas+wadden+sea](https://publicwiki.deltares.nl/display/OET/Dataset+documentation+Sediment+atlas+wadden+sea) (accessed on 6 May 2019).
27. Mondriaankwelder. Restoring and Developing New Salt Marshes with Unique and Innovative Open Salt Marsh Structures. Available online: <https://www.sense-of-place.eu/en/wadland/> (accessed on 23 March 2020).
28. Charnock, H. Wind stress on a water surface. *Q. J. R. Meteorol. Soc.* **1955**, *81*, 639–640. [[CrossRef](#)]



29. Booij, N.; Ris, R.C.; Holthuijsen, L.H. A third-generation wave model for coastal regions: 1. Model description and validation. *J. Geophys. Res. Ocean.* **1999**, *104*, 7649–7666. [[CrossRef](#)]
30. Van Rijn, L.C. *Principles of Sediment Transport in Rivers, Estuaries and Coastal Seas*; Aqua Publications: Amsterdam, The Netherlands, 1993; ISBN 90-800356-2-9.
31. Van Rijn, L.C. *General View on Sand Transport by Currents and Waves: Data Analysis and Engineering Modelling for Uniform and Graded Sand (TRANSPOR 2000 and CROSMOR 2000 Models)*; Z2899; Deltares (WL): Delft, The Netherlands, 2000.
32. Deltares. *Delft3D FM Suite*; D-Flow Manual; Deltares: Delft, The Netherlands, 2019.
33. Dijkema, K.S.; van Duin, W.; Dijkman, E.; Nicolai, A.; Jongerius, H.; Keegstra, H.; Jongsma, J.J. Friese en Groninger kwelderwerken: Monitoring en beheer 1960–2010. *Wettelijke Onderz. Natuur & Milieu* **2013**, *68*. [[CrossRef](#)]
34. Horstman, E.M.; Dohmen-Janssen, C.M.; Bouma, T.J.; Hulscher, S.J. Tidal-scale flow routing and sedimentation in mangrove forests: Combining field data and numerical modelling. *Geomorphology* **2015**, *228*, 244–262. [[CrossRef](#)]
35. Oost, A.P. *Dynamics and Sedimentary Developments of the Dutch Wadden Sea with a Special Emphasis on the Frisian Inlet: A Study of the Barrier Islands, Ebb-Tidal Deltas, Inlets and Drainage Basins*; Faculteit Aardwetenschappen: Utrecht, The Netherlands, 1995.
36. Van Ledden, M.; Van Kesteren, W.; Winterwerp, J. A conceptual framework for the erosion behaviour of sand–mud mixtures. *Cont. Shelf Res.* **2004**, *24*, 1–11. [[CrossRef](#)]
37. Friedrichs, C.T. Tidal Flat Morphodynamics: A Synthesis. *Treatise on Estuarine and Coastal Science: Sedimentology and Geology. Elsevier* **2011**, 137–170. [[CrossRef](#)]
38. Van der Wegen, M.; Roelvink, J. Reproduction of estuarine bathymetry by means of a process-based model: Western Scheldt case study, the Netherlands. *Geomorphology* **2012**, *179*, 152–167. [[CrossRef](#)]
39. Loon-Steensma, J.M.; Slim, P.A.; Vroom, J.; Stapel, J.; Oost, A.P. *Een Dijk van een Kwelder; Een Verkenning naar de Golfreducerende Werking van Kwelders*; Alterra-rapport 2267; Alterra: Wageningen, The Netherlands, 2012.
40. Deltares. *Delft3D FM Suite*; D-Morphology Manual; Deltares: Delft, The Netherlands, 2019.
41. Francalanci, S.; Bondoni, M.; Rinaldi, M.; Solari, L. Ecomorphodynamic evolution of salt marshes: Experimental observations of bank retreat processes. *Geomorphology* **2013**, *195*, 53–65. [[CrossRef](#)]
42. Woth, K.; Weisse, R.; Von Storch, H. Climate change and North Sea storm surge extremes: An ensemble study of storm surge extremes expected in a changed climate projected by four different regional climate models. *Ocean Dyn.* **2006**, *56*, 3–15. [[CrossRef](#)]
43. Deltares. Dataset: Vaklodgingen. RWS, Ed.; 2015. Available online: [Publicwiki.deltares.nl](https://publicwiki.deltares.nl) (accessed on 7 May 2019).
44. NLHO. *Representatief Bathymetrisch Bestand*; van Defensie Ministerie, K.M., der Hydrografie, D., Eds.; Hydrographic Office: The Hague, The Netherlands, 2013; Available online: [Publicwiki.deltares.nl/display/OET/Dataset+documentation+bathymetry+NLHO](https://publicwiki.deltares.nl/display/OET/Dataset+documentation+bathymetry+NLHO) (accessed on 8 May 2019).
45. Zijl, F.; Verlaan, M.; Gerritsen, H. Improved water-level forecasting for the Northwest European Shelf and North Sea through direct modelling of tide, surge and non-linear interaction. *Ocean Dyn.* **2013**, *63*, 823–847. [[CrossRef](#)]
46. Wamsley, T.V.; Cialone, M.A.; Smith, J.M.; Atkinson, J.H.; Rosati, J.D. The potential of wetlands in reducing storm surge. *Ocean Eng.* **2010**, *37*, 59–68. [[CrossRef](#)]
47. Willemsen, P.W.J.M.; Horstman, E.; Borsje, B.W.; Friess, D.; Dohmen-Janssen, C.M. Sensitivity of the sediment trapping capacity of an estuarine mangrove forest. *Geomorphology* **2016**, *273*, 189–201. [[CrossRef](#)]
48. Pope, S.B. *Turbulent Flows*; Cambridge University Press: Cambridge, UK, 2001; Volume 125, pp. 1361–1362.
49. Carrère, L.; Lyard, F.; Cancet, M.; Guillot, A.; Roblou, L. FES 2012: A new global tidal model taking advantage of nearly 20 years of altimetry. In *Proceedings of the 20 Years of Progress in Radar Altimetry*, Venice, Italy, 24–29 September 2013.
50. Wright, J.; Colling, A.; Park, D. *Waves, Tides and Shallow-Water Processes*; Gulf Professional Publishing: Houston, TX, USA, 1999; Volume 4.
51. Li, F.; van Gelder, P.; Ranasinghe, R.; Callaghan, D.; Jongejan, R. Probabilistic modelling of extreme storms along the Dutch coast. *Coast. Eng.* **2014**, *86*, 1–13. [[CrossRef](#)]
52. KNMI. HiRLAM Data Package. 2017. Available online: [Data.overheid.nl](https://data.overheid.nl) (accessed on 5 May 2019).

53. Hasselmann, K.; Barnett, T.P.; Bouws, E.; Carlson, H.; Cartwright, D.E.; Enke, K.; Ewing, J.A.; Gienapp, H.; Hasselmann, D.E.; Kruseman, P.; et al. *Measurements of Wind-Wave Growth and Swell Decay during the Joint North Sea Wave Project (JONSWAP)*, E. 8-12, Editor; Deutsches Hydrographisches Institut: Hamburg, Germany, 1973.
54. Madsen, O.S.; Mathisen, P.P.; Rosengaus, M.M. Movable bed friction factors for spectral waves. In Proceedings of the 22nd International Conference on Coastal Engineering, ASCE, Delft, The Netherlands, 2–6 July 1990; Volume 22, pp. 420–429.
55. Nash, J.E.; Sutcliffe, J.V. River flow forecasting through conceptual models part I—A discussion of principles. *J. Hydrol.* **1970**, *10*, 282–290. [[CrossRef](#)]
56. Willmott, C.J. On the validation of models. *Phys. Geogr.* **1981**, *2*, 184–194. [[CrossRef](#)]
57. Elias, E.P.; Gelfenbaum, G.; Van der Westhuysen, A.J. Validation of a coupled wave-flow model in a high-energy setting: The mouth of the Columbia River. *Geophys. Res.* **2012**, *117*. [[CrossRef](#)]
58. Flemming, B.; Delafontaine, M. Mass physical properties of muddy intertidal sediments: Some applications, misapplications and non-applications. *Cont. Shelf Res.* **2000**, *20*, 1179–1197. [[CrossRef](#)]
59. van Kessel, T.; Boer, A.S.; van der Werf, J.; Sittoni, L.; van Prooijen, B.; Winterwerp, H. *Bed Module for Sand-Mud Mixtures*; Deltares: Delft, The Netherlands, 2012.
60. Zijlema, M.; Van Vledder, G.P.; Holthuijsen, L. Bottom friction and wind drag for wave models. *Coast. Eng.* **2012**, *65*, 19–26. [[CrossRef](#)]



© 2020 by the authors. Licensee MDPI, Basel, Switzerland. This article is an open access article distributed under the terms and conditions of the Creative Commons Attribution (CC BY) license (<http://creativecommons.org/licenses/by/4.0/>).